Biogeosciences
Discussions

Open Access

EGU

Observed and forecasted global warming pressure on coastal hypoxia

Michael M. Whitney[1]

[1]Department of Marine Sciences, University of Connecticut, 1080 Shennecossett Road, Groton, CT, USA

Correspondence to: Michael M. Whitney (michael.whitney@uconn.edu)

5   **Abstract.** Coastal hypoxia is a major environmental problem of increasing severity. A global 40-year observational gridded climate data record and 21st century forecasts from the Community Earth System Model under RCP 8.5 forcing are analyzed for long-term linear trends with a focus on warming-related pressures on coastal oxygen conditions. The forecasted median trends along the global coast are 0.32 °C, -1.6 mmol m^{-3}, and -1.2 mmol m^{-3} per decade for sea-surface temperature (SST), surface oxygen capacity, and vertical-minimum oxygen concentration, respectively. These trends point to more rapid
10   deterioration in coastal conditions than experienced over the last four decades; the forecasted median coastal trends for SST and oxygen capacity are 48% and 18% faster than the corresponding observed rates. Median rates for the coast and documented hypoxic areas are higher than in the global ocean. Warming and oxygen declines tend to be fastest at high latitudes, one region where new hypoxic areas may emerge as oxygen conditions deteriorate. Over 19% of the coast has extremely rapid forecasted change upwards of 0.60 °C per decade warming and -3.0 mmol m^{-3} per decade oxygen change. There is considerable pressure
15   on current hypoxic areas since future oxygen declines of any magnitude will make hypoxia more severe. The coastal forecasts can inform coastal environmental management strategies to protect future water quality and ecosystem services.

1 Introduction

Hypoxia in coastal waters is a major environmental problem of increasing severity confronted around the world (Hoegh-Guldberg et al., 2018). "Dead zones in the coastal oceans have spread exponentially since the 1960s and have serious
20   consequences for ecosystem functioning" (Diaz and Rosenberg, 2008). To date, over 500 hypoxic areas in estuaries, coastal seas, and on continental shelves have been documented globally (Breitburg et al., 2018). Furthermore, the severity of hypoxia has increased in many areas (Rabalais et al., 2010). Oxygen concentrations have been decreasing an order of magnitude faster than surface-layer concentrations in the open ocean (Gilbert et al., 2010). Worsening coastal oxygen conditions are attributable to the dual human pressures of nutrient overloading fueling eutrophication and anthropogenic climate change (e.g. Rabalais
25   and Turner, 2001; Paerl, 2006; Diaz and Rosenberg, 2011). Coastal oxygen conditions are influenced by many aspects of climate controls including warming waters, altered storm patterns, changing precipitation and river flow, sea-level rise, ocean acidification, and shifting ocean circulation (Altieri and Gedan, 2015). This paper focuses on warming-related pressures on coastal hypoxia. Oxygen capacity (oxygen saturation concentration) decreases with increased water temperatures (Weiss, 1970; Garcia and Gordon, 1992), which can exacerbate hypoxia. Furthermore, metabolic rates and related oxygen demands

30   rise with temperature (Brown et al., 2004). Warming also can intensify and extend the duration of summertime thermal
stratification that inhibits ventilation of near-bottom hypoxic waters (Cloern, 2001).

Earth system models provide forecasts of 21st century conditions relevant to coastal hypoxia. Altieri and Gedan (2015)
analyzed sea surface temperature (SST) forecasts from the Community Climate System Model (Collins et al., 2006) for the
greenhouse gas emissions A1B scenario (Nakicenovic and Swart, 2000). Under this emission scenario, almost all known

35   coastal hypoxic areas (based on the Diaz and Rosenberg (2008) dataset) would experience 2 °C or greater water temperature
rise by the century end (Altieri and Gedan, 2015). There is a need to update this type of analysis with more recent climate
modeling. The present study analyzes Community Earth System Model (CESM) results for the Representative Concentration
Pathway (RCP) 8.5 (Moss et al., 2010). The RCP 8.5 exhibits more global warming than the earlier A1B emission scenario
(Melillo et al., 2014).

40   Earth system models offer great value in forecasting future conditions, but they do have limitations that affect coastal
applications. The relatively course horizontal and bathymetric resolution of CESM and most Earth system models, particularly
those including ocean biogeochemistry, limits the representation of coastal processes. Earth system models do not currently
resolve estuary ecosystems, but they do have the resolution to represent coastal conditions at regional scales. Regional patterns
strongly influence rates of change for coastal SST (e.g. Pershing et al., 2015) and temperature-related changes in oxygen

45   capacity. Coastal oxygen concentrations should vary with the regional variations in temperature and oxygen capacity resolved
by Earth system models, but oxygen levels also depend on other abiotic and biotic factors. Oxygen concentrations tend to be
highly variable on small spatial scales that are not resolved by CESM, particularly within estuarine waters. For these reasons,
it is likely that forecasted changes for coastal oxygen concentrations are less reliable than SST and oxygen capacity. Open-
ocean results at 300 m (Oshlies et al., 2017) and 100-600 m (Cocco et al., 2013) point to model limitations in representing the

50   observed distribution of dissolved oxygen trends. It is reasonable to expect model-observation mismatches also occur in open-
ocean surface waters and along coasts. The forecasts for temperature and oxygen changes, nevertheless, are worth considering
given the importance of anticipating potentially worsening conditions in coastal hypoxic areas. Forecasts from Earth system
models should be considered in the context of observed trends in coastal conditions and compared to available global coastal
observations. Gridded SST climate data records can provide sufficient global coastal data coverage and allow for computation

55   of oxygen capacities to evaluate whether Earth system models provide reasonable representations of coastal conditions
affecting hypoxia.

The main objective of this paper is studying global patterns exacerbating coastal hypoxia by analyzing linear trends in SST,
surface oxygen capacity, and (vertical-minimum) oxygen concentration. Observations from a satellite-derived SST global
climate data record (Merchant et al., 2019; Embury and Good, 2021) are analyzed for coastal SST and oxygen-capacity trends

60   over the last four decades, which provide context for forecasts. New analysis of 21st century forecasts from the CESM Large
Ensemble Project (Kay et al., 2015a,b) is completed for coastal areas and compared to open-ocean rates. Observed and
forecasted coastal SST and oxygen capacities are compared for the first 16 years of the forecast period that already have
occurred. The study not only investigates forecasts for documented coastal hypoxic locations, but also considers the entire

global coast to include unknown and potentially emerging hypoxic areas. Results are placed in the context provided by other

65   studies and the implications for future coastal hypoxia are discussed.

2 Methods

2.1 Observations

The global observational dataset analyzed is the satellite-based SST time-series described in Merchant et al. (2019) and available with updates at the Climate Data Store of the Copernicus Climate Change Service (Embury and Good, 2021). The

70   Level-4 (version 2.0) product combines SST data from several satellite platforms to construct a high-quality climate data record. The dataset is a daily product on a regular grid with 0.05° (latitude and longitude) resolution. The Level-4 product is gap-filled so that each grid point has an SST value for every day from September 1981 up to within a month of present time. This study analyzes 40 years of data spanning 1982-2021. Daily data during each August and February are used to represent summer conditions in the northern and southern hemispheres, respectively. The rationale for analyzing these months is they

75   are the summer months in each hemisphere when water temperatures tend to be highest and oxygen levels tend to be lower. Daily data are averaged to create August-averaged and February-averaged SST time series for the northern and southern hemispheres, respectively. Oxygen capacity is calculated with the Garcia and Gordon (1992) oxygen saturation concentration equations using the monthly averaged SST data and a constant 35 salinity. The constant salinity is used because the Merchant et al. (2019) product does not include salinity and because this straightforward approach is sufficient to provide observational

80   context for forecasts. Coastal points are defined as grid points with at least on neighboring land cell (directly to the east, west, north, or south). Techniques for comparing observations to forecasts for overlapping years, for calculating observed linear trends, and extracting information at documented hypoxic areas are described in subsequent sections.

2.2 Forecasts

Forecasts of 21st century water temperatures and oxygen conditions are derived from the CESM Large Ensemble Project that

85   includes ocean biogeochemistry (Kay et al., 2015a), which is a contributor to Climate Model Intercomparison Project phase 5 (CMIP5, Taylor et al., 2012). Monthly-averaged results for 2006-2100 are accessed via the Earth System Grid (Kay et al., 2015b). Multiple ensemble members for RCP 8.5 forcing (following CMIP5 protocols) are used: 35 and 27 ensemble members for SST and oxygen capacity, respectively. Runs 1-35 for SST (the "SST" variable) and runs 1, 2, and 9-35 for surface oxygen saturation concentration (the "O2SAT" variable) and vertical-minimum oxygen concentration (the "O2_ZMIN" variable).

90   Runs 3-8 are omitted for O2SAT and O2_ZMIN because these results are not available on the Earth System Grid. Additional runs (101 and higher) were avoided because of a documented unexplained positive bias in global temperature relative to other ensemble members. All included runs are averaged together to produce ensemble-mean monthly time series of SST, surface oxygen saturation concentration (oxygen capacity), and vertical-minimum oxygen concentrations at each ocean grid cell.

For each year at each CESM ocean grid cell (at 1° latitude nominal resolution), the month with minimum surface oxygen
95   saturation concentration is selected to construct annual time series of minimum oxygen capacity and coincident SST and
vertical-minimum oxygen concentrations. August and February are the median months associated with minimum surface
oxygen capacity in the northern and southern hemispheres, respectively. The global set of all coastal points includes all CESM
ocean grid cells with at least one neighboring land cell (there are 4,899 coastal cells). Coastal points are defined as grid points
with at least on neighboring land cell. Globally, there are 4,899 cells coastal cells. Techniques for comparing forecasts and
100 observations for overlapping years, for calculating forecasted linear trends, and extracting information at documented hypoxic
areas are described in the following sections.

2.3 Comparison of observations and forecasts

To characterize the reliability of CESM in coastal areas, observations and forecasts are compared for global coastal points.
There are 16 forecast years spanning 2006-2021 that now overlap with observed conditions. Every CESM coastal point is
105 matched with the closest coastal point on the observational grid, which has higher spatial resolution than the forecast grid. The
summer month values (calculated as described in previous section) for the overlapping period are averaged together to
determine mean observed and forecasted values at each coastal point. The resulting SST and oxygen capacity values are
quantitatively compared to each other. Linear regression is completed to indicate the global relationship between observed and
forecasted SST and oxygen capacity for coastal waters. Regression results are included in the supporting dataset (Whitney,
110 2021) and are reported with the slope, offset, p-value (p) of the F-statistic, correlation coefficient squared (r^2), and root mean
square error (RMSE). The level of agreement between observed and forecasted mean values for the overlapping period assesses
the quality of CESM performance in coastal waters. Observed and forecasted temporal trends are not compared for the
overlapping period because observations have high interannual variability that can obscure longer-term trends over shorter
periods. Individual ensemble members have comparably large interannual variability, but the ensemble-mean forecast results
115 have much less interannual variability.

2.4 Trend analysis

Linear regression analysis is applied to characterize long-term temporal trends. For observations, the entire 40-year
observational period is regressed with time for SST and surface oxygen capacity. For forecasts, the entire 94-year forecast
period is regressed for SST, surface oxygen capacity, and oxygen concentrations. The regression slopes are reported as rates
120 of change associated with each variable and are included in the supporting dataset (Whitney, 2021). Regression statistics are
calculated. The p-values of the F-statistic are used to categorize results depending on whether or not they are statistically
significant at the 90% confidence level (p=0.10). Correlation coefficients are calculated but not emphasized because ensemble-
mean forecasts average out interannual variability present in ensemble members and therefore tend to have high r^2 values;
while the observational record has higher interannual variability and correspondingly lower r^2 values. Rates of change are

125   shown for the entire global ocean and emphasis is placed on change in coastal waters. The documented coastal hypoxic areas
are further highlighted and are identified as described in the next section.

2.5 Documented coastal hypoxic areas

The 532 documented coastal hypoxic areas analyzed are from the Diaz et al. (2011) database. The dataset is an expanded
version of the Diaz and Rosenberg (2008) database, which is similar to the coastal dataset in Breitburg et al. (2018). The

130   oxygen concentration threshold used to identify hypoxia in the dataset is 63 mmol m^{-3} (2 mg L^{-1}) (Diaz and Rosenberg, 2008).
The Diaz et al. (2011) database also includes 244 additional locations classified as eutrophic (but not hypoxic) that are not
included in this analysis. Rates of change (for SST, oxygen capacity, and oxygen concentration) for the documented hypoxic
areas are extracted from rates at the nearest observational coastal grid point or CESM coastal ocean grid cell. The observational
grid resolution is fine enough to represent each individual documented coastal hypoxic area with a separate observational grid

135   point. The coarser (nominally 1 º latitude) CESM resolution causes some documented locations to be represented by the same
CESM coastal cell. The 532 documented locations map to only 240 unique CESM ocean grid cells.

3 Results

3.1 Observed trends

The 40-year observational SST record (updated from Merchant et al., 2019) indicates warming has occurred throughout the

140   world ocean (Fig. 1a). SST rates are stronger in the Northern Hemisphere, with the most rapid warming occurring in Arctic
areas near coasts. Just over half (55%) of the ocean grid points have linear trends with p≤0.10 (Table 1). P-values are lower
where calculated rates are lower in parts of the Atlantic, much of the South Pacific, and most of the Southern Ocean. Where
p≤0.10, the mean r^2=0.20; indicating that linear trends describe an appreciable part of the observed variance, but interannual
variability is larger. The observed global median SST trend (including only points with p≤0.10) is 0.22 ºC per decade (Table

145   1). The median trend with all points included (regardless of p-value) is 0.13 ºC per decade. This rate is consistent with the
global mean SST rate of 0.1ºC per decade from 1982-2013 (Pershing et al., 2015).

Observed rates along the global coast indicate conditions relevant to coastal hypoxia. The median SST trend for global coastal
points (0.27 ºC per decade, for points with p≤0.10) is 22% faster than the observed ocean median rate (Table 1). SST rates
tend to be near the median coastal value from 60 ºS to 30 ºN (Fig. 1b) and increase towards higher latitudes. The observed

150   median trend for documented hypoxic areas (0.24 ºC per decade) is 6% faster than the ocean median rate (Table 1), but is
lower than the median global coastal rate because there are few documented hypoxic areas at high latitudes where warming is
fastest. The histograms of SST rates (Fig. 1c) indicate the documented hypoxic areas have a narrower spectrum than the global
coastal points.

The global distribution of oxygen capacity (saturation concentration) trends (Fig. 2a) at the surface is tied to observed SST

155   rates (Fig. 1a). Since oxygen saturation concentrations decrease nonlinearly with temperature with a greater response at lower
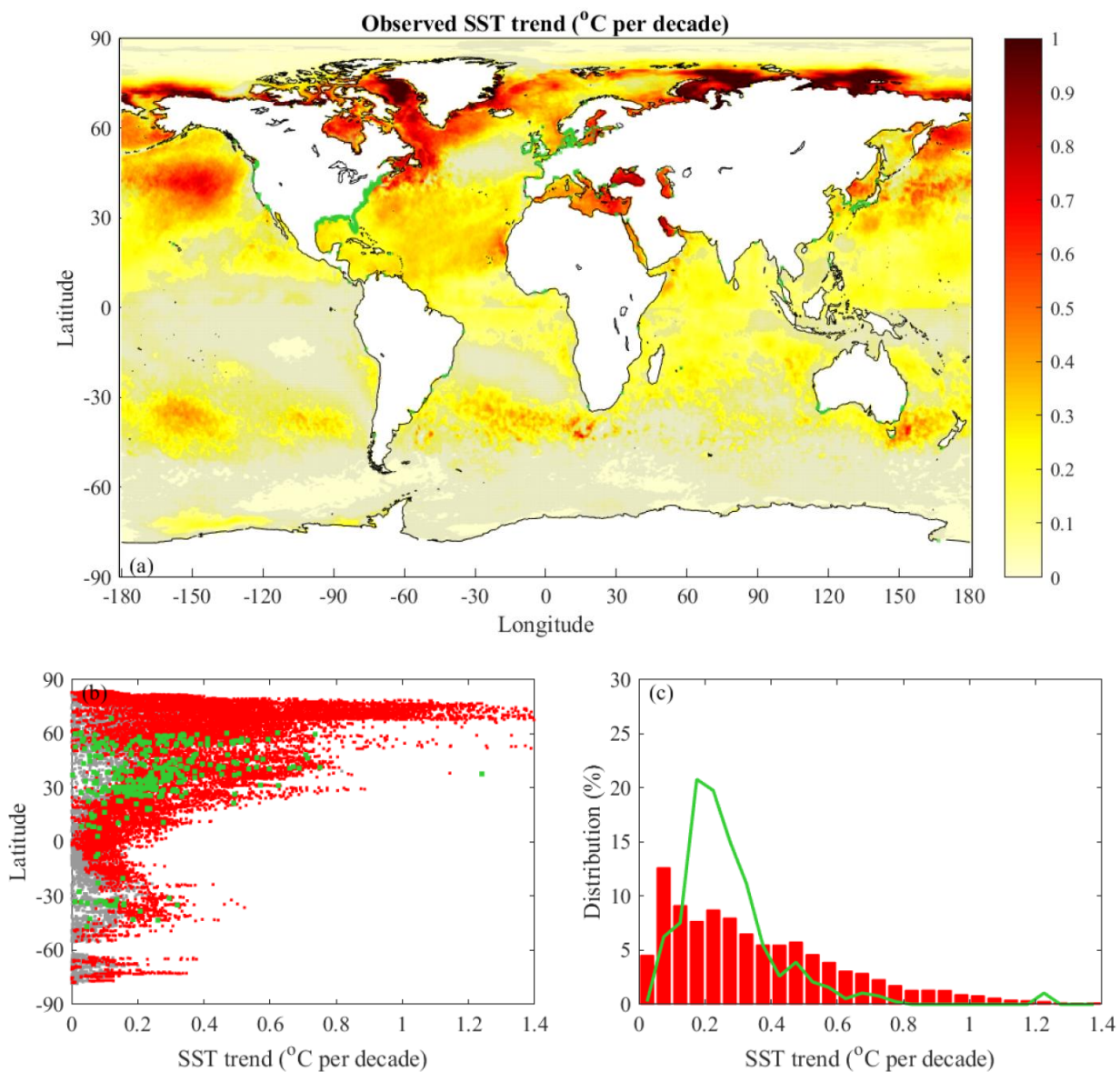
Figure 1: Observed SST trends: (a) spatial distribution for all ocean observational points, (b) latitudinal dependence for global coastal points and documented coastal hypoxic areas, and (c) histograms of global coastal points and documented coastal hypoxic areas (having linear trends with p≤0.10). Locations that have linear trends with lower confidence (p>0.10) are marked with gray points. Global coastal data are shown as red points and bars. Documented coastal hypoxic areas are marked in green.

temperatures, oxygen capacity decreases are amplified at high latitudes where waters are colder and forecasted warming rates are faster (Weiss, 1970; Garcia and Gordon, 1992; Altieri and Gedan, 2015). Oxygen capacity linear trends with p≤0.10 occur in the same locations as for SST trends and r^2 values are similar to those for SST. The observed global median oxygen capacity trend at the surface (including only points with p≤0.10) is -0.9 mmol m^{-3} per decade (Table 1). This rate is several times faster

Table 1: Observed (1982-2021) and forecasted (2006-2100) median linear trends in SST, surface oxygen capacity, and vertical-minimum oxygen concentrations (forecasted only) for the ocean, global coastal cells, and documented coastal hypoxic areas. All points included in median calculations have linear trends with p≤0.10, the corresponding percent coverage of p≤0.10 is given in square brackets.

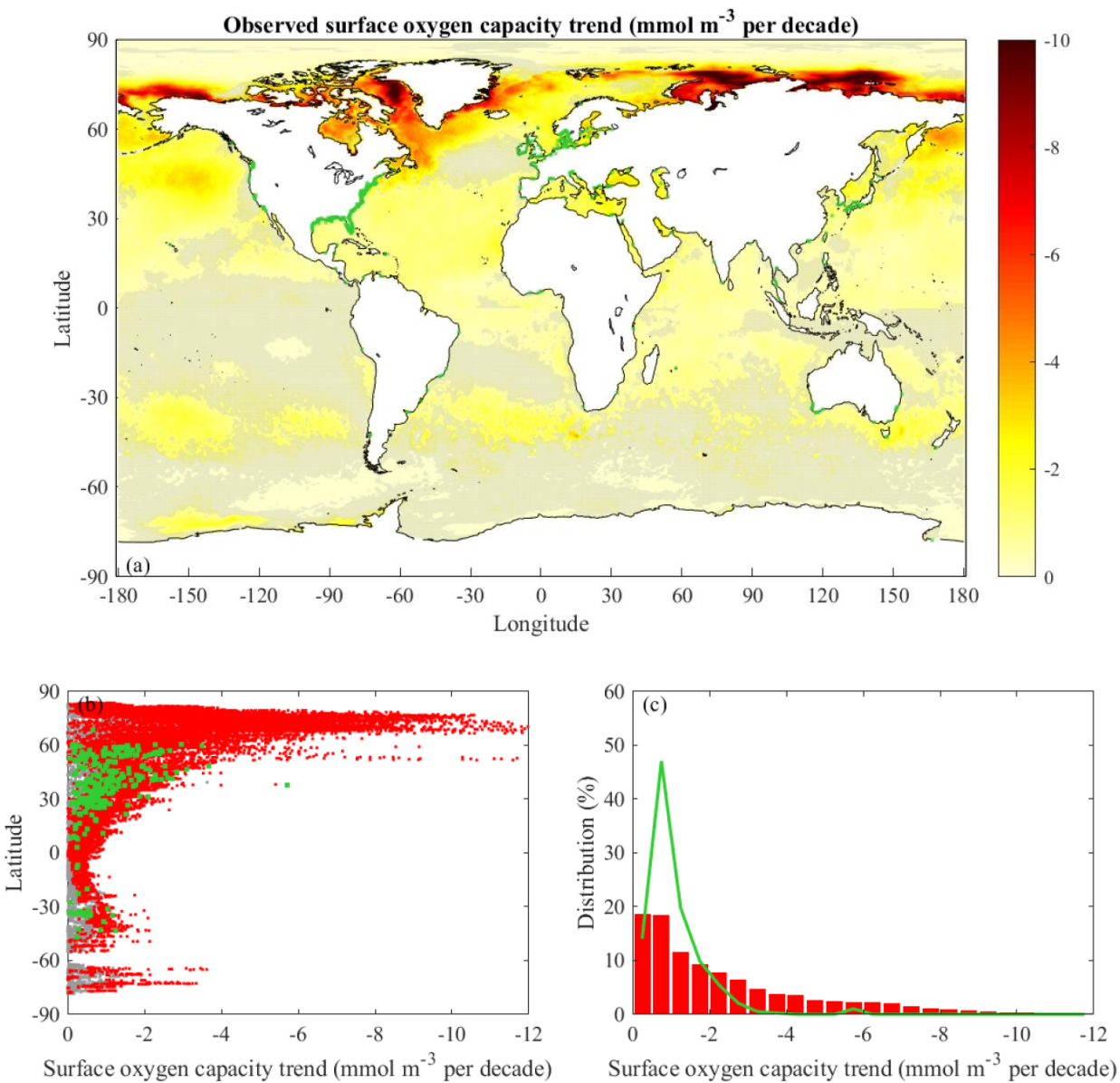| Rate	Ocean	Coastal	Hypoxic
Observed SST (°C per decade)	0.218 [55.12%]	0.265 [70.64%]	0.236 [76.13%]
Observed oxygen capacity (mmol m^{-3} per decade)	-0.82 [55.06%]	-1.34 [70.64%]	-0.78 [76.13%]
Forecasted SST (°C per decade)	0.352 [100%]	0.392 [100%]	0.402 [100%]
Forecasted oxygen capacity (mmol m^{-3} per decade)	-1.23 [100%]	-1.58 [99.98%]	-1.39 [100%]
Forecasted oxygen conc. (mmol m^{-3} per decade)	-0.65 [97.24%]	-1.15 [97.39%]	-1.38 [100%]

170   than the median rate of -0.2 mmol m^{-3} per decade observed in offshore (farther than 100 km from the coast) upper-ocean (0-300 m depth) waters for 1976-2000 (Gilbert et al., 2010).

The observed median oxygen capacity trend for global coastal points (-1.4 mmol m^{-3} per decade, for points with p≤0.10) is 62% faster than the surface ocean median rate (Table 1). The observed median coastal rate is half of the rate calculated for a global coastal band (within 30 km of the coast) for 1976-2000 (Gilbert et al., 2010). Rates tend to be near the median coastal

175   value from 60 °S to 30 °N (Fig. 2b). At higher latitudes, rates tend to increase with latitude. The median oxygen capacity trend for documented hypoxic areas is -0.8 mmol m^{-3} per decade (Table 1). This rate is lower magnitude than for all global coastal points because of little high-latitude coverage, where oxygen capacity rates are largest. Similar to SST rates, the histograms for oxygen capacity (Fig. 2c) indicate the documented hypoxic areas have a narrower spectrum than the global coastal points. Overall, the observational SST and oxygen capacity analysis provides context for the forecasts and new information about

180   global coastal conditions influencing coastal hypoxia.
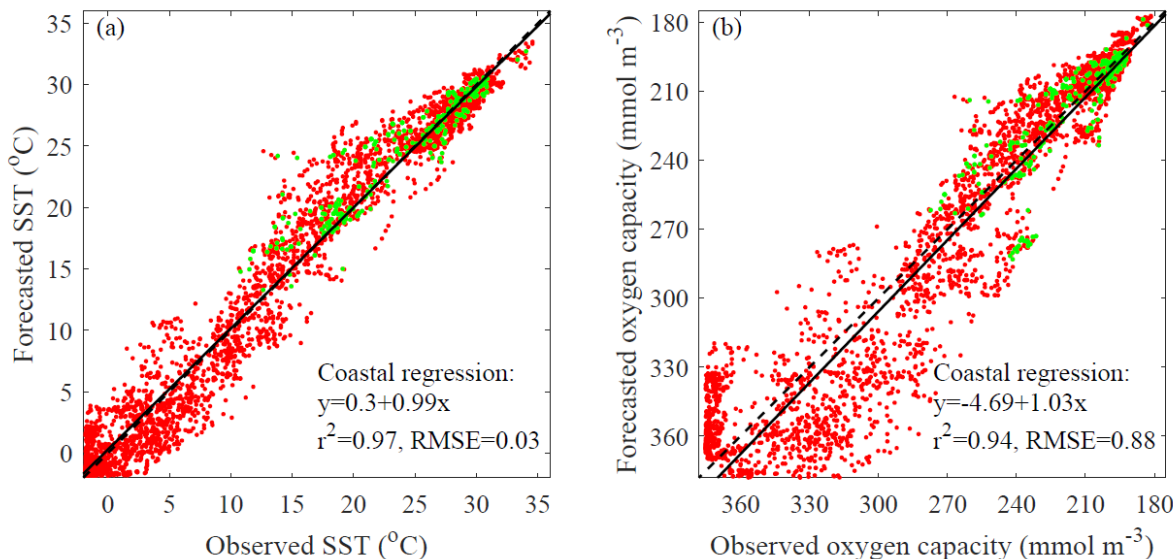
3.2 Comparison of observations and forecasts

The observational SST record is compared to CESM forecasted coastal conditions for the overlapping 16 years spanning 2006-2021 (Fig. 3a). There is an essentially one-to-one relationship between observed and forecasted coastal SST with a low p-value (p<0.001) and high correlation (r^2=0.97). There is approximate 5 °C scatter around the linear relationship, but the RMSE is

185   small (0.03 °C). This level of agreement indicates that CESM results are broadly representative of global coastal SST conditions. The comparison of observed and forecasted coastal oxygen capacities averaged over the overlapping period (Fig. 3b) show a near one-to-one relationship with a low p-value (p<0.001) and high correlation (r^2=0.94). The scatter away from the regression line is larger at higher oxygen capacities (in colder waters). The nonlinear relationship between temperature and oxygen capacity (noted above) means that temperature scatter in colder waters translates into more oxygen capacity scatter.

190   This analysis points to the degree of reliability of CESM results for representing coastal oxygen capacities. Overall, the comparison of observations and CESM results suggest that CESM can provide reliable forecasts of coastal conditions relevant to coastal hypoxia.

195

Figure 2: Observed surface oxygen capacity (saturation concentration) trends: (a) spatial distribution for all ocean observational points, (b) latitudinal dependence for global coastal points and documented coastal hypoxic areas, and (c) histograms of global coastal points and documented coastal hypoxic areas. The format and color coding follow Fig. 1.

Figure 3: Comparison of forecasted to observed coastal conditions: (a) SST and (b) surface oxygen capacity. Mean values for the overlapping 2006-2021 period are compared. Global coastal points and documented coastal hypoxic areas are marked in red and green, respectively. The one-to-one line (dashed) and linear regression (solid) are included along with associated regression statistics (p<0.001 for both regressions).

3.3 Forecasted trends

The CESM Large Ensemble Project ensemble-mean forecast for the RCP 8.5 scenario indicates SST will appreciably increase throughout the world ocean over the 21st century (Fig. 4a). All of the ocean cells have linear trends with p≤0.10 (Table 1). SST rates account for more than 90% of the variance in the ensemble-mean forecast (r^2>0.90) for most of the ocean; the only exceptions are some areas to the north and south of Greenland and near parts of Antarctica. The forecasted global median SST trend is 0.35 °C per decade (Table 1). Global distributions of SST warming have been studied in detail for multiple models and RCP scenarios (e.g. Bopp et al., 2013). Bopp et al. (2013) includes CESM simulations in an analysis of ten models running the RCP 8.5 scenario and finds the global average SST increase is 0.27 °C per decade (from the 1990s to 2090s) when averaged across all included models. The CESM forecasted global median SST trend is 61% higher than the observed global warming rate (0.22 °C per decade) calculated in the previous section (Table 1). Under the RCP 8.5 scenario, the ocean SST will increase considerably faster than the observed linear trend over the last four decades.

The global distribution of SST warming indicates variations among oceans, with the Arctic Ocean forecasted to experience at least twice the median warming rates (Fig. 4a). The influence of ocean circulation patterns on warming rates also is evident. Observations (Fig. 1a) also indicate rapid SST increases near Arctic coasts and influences of ocean circulation are evident. There are, however, clear differences in the spatial structure of forecasted and observed rates. Differences away from the coast
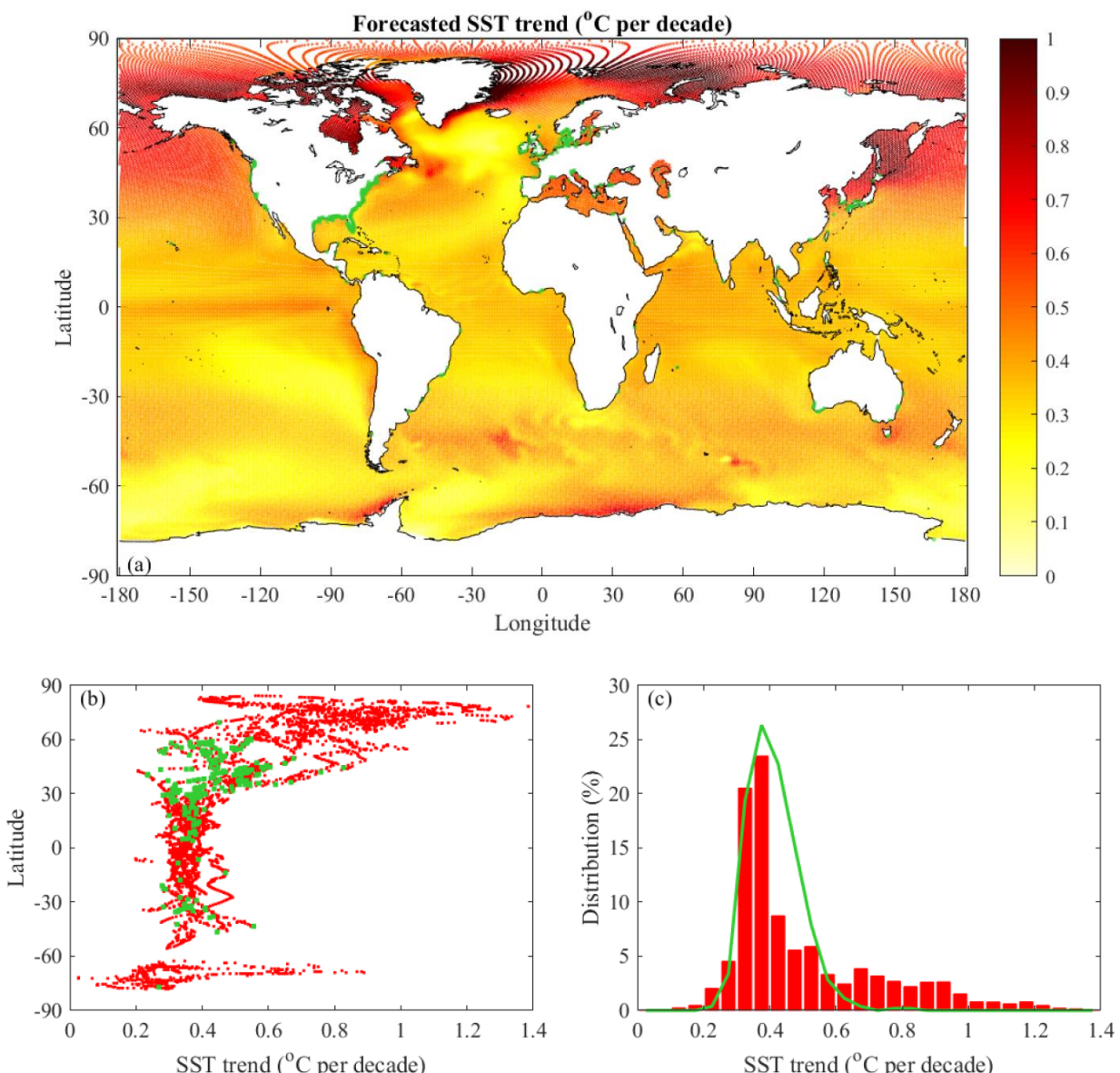
Figure 4: Forecasted SST trends: (a) spatial distribution for all CESM ocean grid cells, (b) latitudinal dependence for global coastal points and documented coastal hypoxic areas, and (c) histograms of global coastal points and documented coastal hypoxic areas. The format and color coding follow Fig. 1.

in the Arctic Ocean are immediately apparent. The low p-values of observed SST trends in much of the Southern Ocean (p>0.10) preclude comparisons of forecasted and observed spatial structure in this region.

Focusing on warming in global coastal areas reveals new information directly relevant to coastal hypoxia. The forecasted median SST trend for global coastal points (0.39 °C per decade) is 11% faster than the forecasted ocean median rate and 48% higher than the observed median coastal rate (Table 1). SST rates tend to be near the median coastal value from 60 °S to 30 °N

(Fig. 4b). Above 30 °N, warming rates tend to increase with latitude and variability among coasts increases. The latitudinal

230 patterns are broadly similar for forecasted and observed coastal SST rates (Fig. 4b and Fig. 1b). The forecasted median SST trend for documented hypoxic areas (0.40 °C per decade) is 14% faster than the forecasted ocean median rate (Table 1). For documented hypoxic areas, the forecasted median trend is 70% higher than the median observed rate (Table 1) and 75% faster than the median trend under moderate A1B emissions scenario (Altieri and Gedan, 2015). The documented hypoxic areas sample much of the variability in coastal SST rates from 45 °S to 60 °N. The hypoxic area database, however, has little coverage

235 at higher latitudes, where the most rapid warming is forecasted. Histograms (Fig. 4c) indicate most coastal locations (92%) and documented hypoxic areas (96%) are forecasted to warm more than 0.3 °C per decade; 0.1 °C per decade faster than the A1B results in Altieri and Gedan (2015). A significant portion of the global coast (18%) are forecasted to warm faster than 0.6 °C per decade, but few of the documented hypoxic sites (2%) are in this range because most are not at high latitudes.

The global distribution of forecasted oxygen capacity (saturation concentration) trends (Fig. 5a) at the surface is tightly linked

240 to SST rates (Fig. 4a). All of the ocean cells have linear trends with $p \leq 0.10$ (Table 1). The forecasted oxygen capacity trends have $r^2 > 0.90$ over most of the ocean with exceptions in the areas where SST rates have $r^2 \leq 0.90$. The forecasted global median oxygen capacity trend at the surface is -1.2 mmol m^{-3} per decade (Table 1). This rate is 50% higher than the observed global median trend (Table 1). The forecasted median rate for ocean waters above 60 °N (-5.3 mmol m^{-3} per decade) is several times higher than the total ocean median rate.

245 The forecasted median oxygen capacity trend for global coastal points (-1.6 mmol m^{-3} per decade) is 28% faster than the surface ocean median rate (Table 1). The forecasted median coastal rate is 18% faster than observed. Rates tend to be near the median value from 30 °S to 30 °N (Fig. 5b). Outside that latitude range, rates tend to increase with latitude and variability among coasts increases, particularly in the northern hemisphere where rates can exceed -10.0 mmol m^{-3} per decade. The latitudinal pattern in coastal oxygen capacity trends (Fig. 5b) is similar to the observed coastal pattern (Fig. 2b). The median

250 oxygen capacity trend for documented hypoxic areas is -1.4 mmol m^{-3} per decade (Table 1). This rate is lower magnitude than for all global coastal points because of little high-latitude coverage, where oxygen capacity rates are largest. The forecasted median trend for documented hypoxic areas is 78% higher than observed (Table 1). Histograms (Fig. 5c) indicate for most coastal locations (95%) and all documented hypoxic areas the oxygen capacity trend is forecasted to be faster than -0.9 mmol m^{-3} per decade. A significant portion of the global coast (28%) has forecasted rates faster than -3.0 mmol m^{-3} per decade, but

255 few of the documented hypoxic sites (4%) are in this range because most are not at high latitudes.

The forecasted global distribution of vertical-minimum oxygen concentration changes (Fig. 6a) is influenced by warming, oxygen capacity declines, ocean circulation changes (including vertical exchange), and ecosystem changes. In CESM and in nature, the depth of the vertical-minimum oxygen concentration tends to be near-bottom in coastal areas and is bathymetrically constrained to be relatively close to the surface, whereas the minimum oxygen concentration can occur much deeper in the

260 open ocean and consequently have a more remote connection to surface oxygen capacity. The forecasts for most ocean cells have linear trends with $p \leq 0.10$ (Table 1). The global median trend in oxygen is -0.7 mmol m^{-3} per decade (Table 1). The global distribution of vertical-minimum oxygen concentration rates (Fig. 6a) is broadly consistent with the global distribution of the
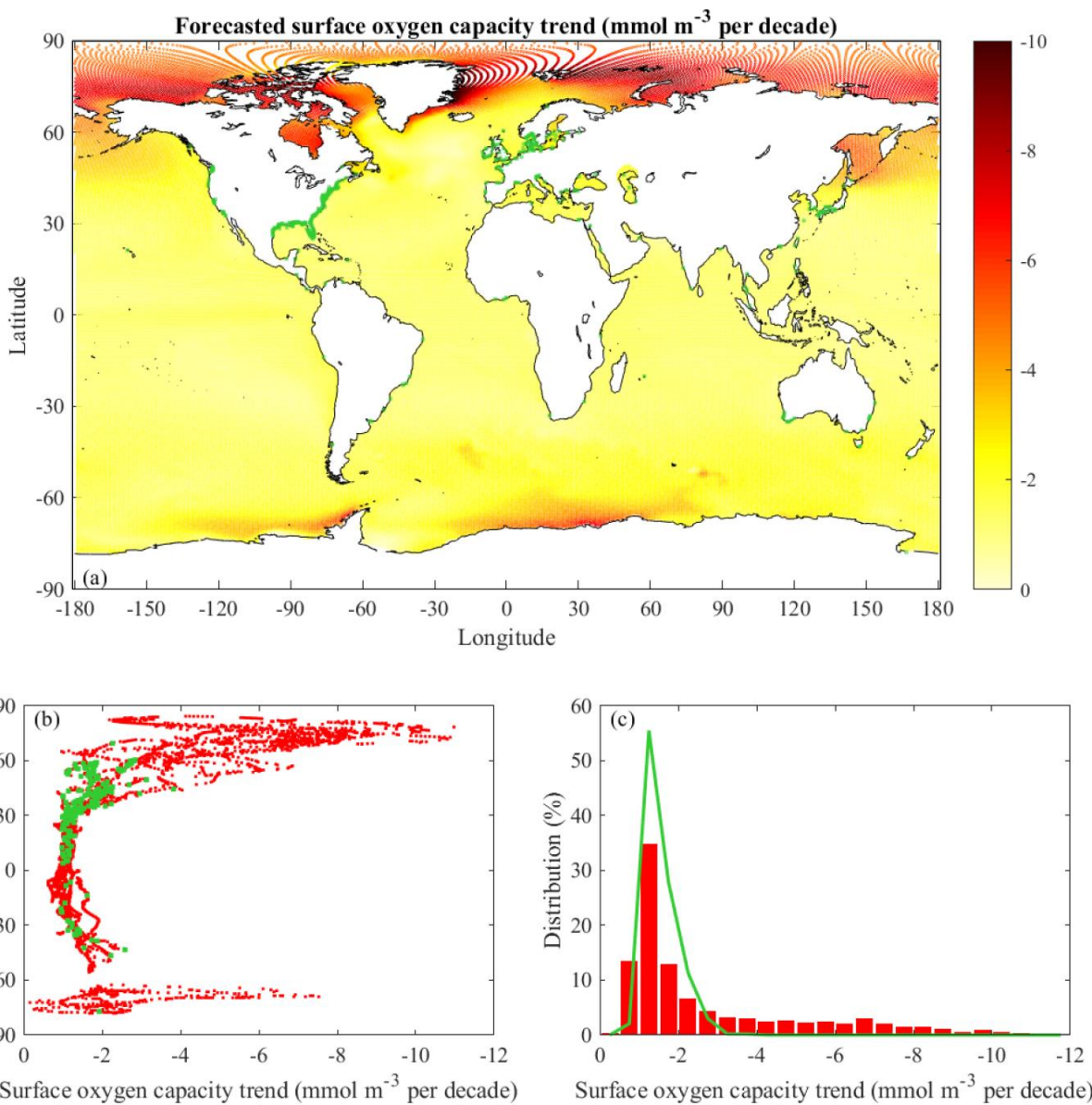
Figure 5: Forecasted surface oxygen capacity (saturation concentration) trends: (a) spatial distribution for all CESM ocean grid cells, (b) latitudinal dependence for global coastal points and documented coastal hypoxic areas, and (c) histograms of global coastal points and documented coastal hypoxic areas. The format and color coding follow Fig. 1.

RCP 8.5 model-average forecasted changes in oxygen concentrations (at 200-600 m depth) shown in Bopp et al. (2013). The total ocean oxygen content decrease (from the 1990s to 2090s) calculated in Bopp et al. (2013) translates to a -0.6 mmol m^{-3} per decade trend, which is close to the current results.

The median trend in vertical-minimum oxygen concentrations for global coastal points (-1.2 mmol m^{-3} per decade) is 77%

faster than the ocean median rate (Table 1). Similar to oxygen capacity, oxygen concentrations rates tend to be near the median

value from 30 °S to 30 °N and increase at higher latitudes (exceeding exceed -10.0 mmol m^{-3} per decade), but there is a lot of

275   scatter (Fig. 6b). The median trend for documented hypoxic areas (-1.4 mmol m^{-3} per decade) is lower than for all global points
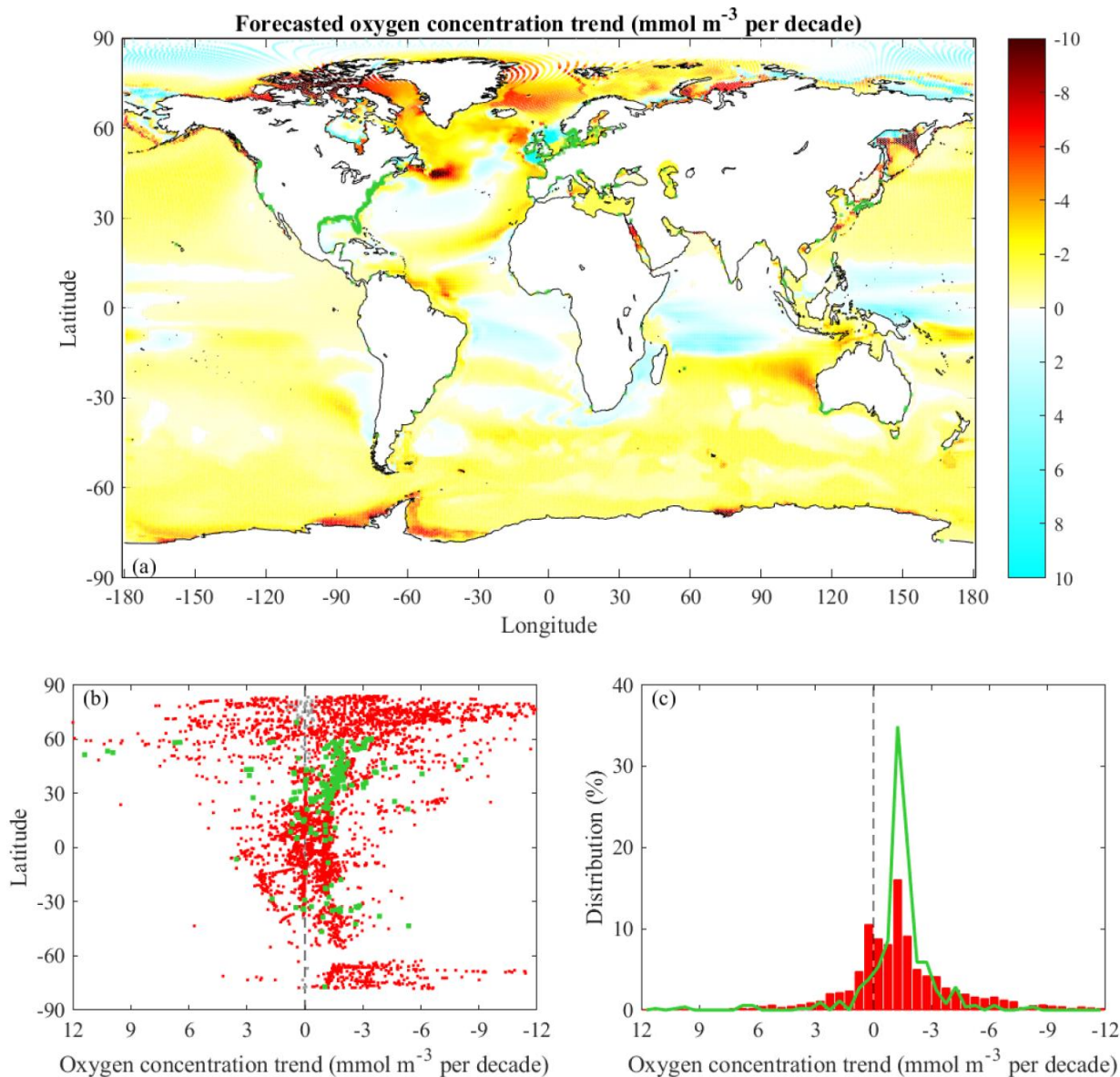

Figure 6: Forecasted vertical-minimum oxygen concentration trends: (a) spatial distribution for all CESM ocean grid cells, (b) latitudinal dependence for global coastal points and documented coastal hypoxic areas, and (c) histograms of global coastal points

280   and documented coastal hypoxic areas. The format and color coding follow Fig. 1 except for the blue shading indicating increasing oxygen concentrations.

because of little high-latitude coverage and approximately the same as the corresponding oxygen capacity decrease (Table 1). Histograms (Fig. 6c) indicate most coastal locations (72%) and documented hypoxic areas (89%) have forecasted oxygen concentration declines. Some coastal (19%) and documented hypoxic areas (8%) have forecasted trends faster than -3.0 mmol

285   m^{-3} per decade.

4 Discussion

The forecasted warming and declining oxygen conditions will exert considerable pressure on current hypoxic areas. The documented hypoxic areas already experience oxygen concentrations at or below the 63 mmol m^{-3} threshold (applied in Diaz and Rosenberg, 2008). If concentrations were at this threshold in 2000, the forecasted median trend in oxygen capacity and

290   concentration represents a 20% reduction by 2100. Furthermore, future oxygen declines of any magnitude will have deleterious ecosystem effects as hypoxia worsens (in intensity and duration) in existing hypoxic areas. The forecasted oxygen declines can erode oxygen gains achieved in systems improved by wastewater treatment and nutrient management. For example, oxygen conditions in Long Island Sound have improved with reduced nutrient loading, but current and forecasted future warming favor deteriorating oxygen conditions (Whitney and Vlahos, 2021).

295   Declines in oxygen conditions along the global coast will create emerging hypoxic areas. Forecasted warming and oxygen declines are particularly severe at high latitudes in the northern hemisphere. Two adjacent fjords in Norway (Trysfjord and Ofotfjord) are the only sites above the Arctic circle within the documented hypoxic area database (Dommasnes et al., 1994; Diaz et al., 2011), but it is likely new Arctic coastal hypoxic areas will emerge. For instance, recent observations suggest Jago Lagoon, Alaska may be on the brink of hypoxia (Smith, 2012; Beaufort Lagoon Ecosystems LTER, 2020). High-latitude

300   waters are colder and therefore tend to have higher saturation concentrations farther from the hypoxic threshold, but oxygen conditions are forecasted to decline most rapidly in these coastal waters. Emphasis also should be placed on rapidly growing coastal megacities at low and mid-latitudes, which tend to struggle with wastewater treatment infrastructure as populations increase and are likely to experience emerging or worsening hypoxia (von Glasow et al., 2013; Varis et al., 2006).

It is important to note that ecosystem problems can arise before conditions deteriorate down to the canonical hypoxic threshold

305   (63 mmol m^{-3}), as many organisms experience physiological stresses above this threshold and have differing tolerances for low oxygen conditions (Vaquer-Sunyer and Duarte, 2008). In addition to directly reducing oxygen capacities, warming also increases metabolic rates, related biological oxygen demand, and thermal stratification (Brown et al., 2004; Cloern, 2001; Breitburg et al., 2018). Thus, attention should be paid to all coastal areas with lowering oxygen conditions, not just the areas already experiencing seasonal hypoxia.

310   The results of this study provide a global perspective on some of the climate pressures confronting existing and emerging coastal hypoxic areas. Observations indicate the warming and reduced oxygen capacities that coastal waters have been experiencing and the CESM forecast for the RCP 8.5 scenario points to even more rapid warming and oxygen declines throughout the 21st Century. It is encouraging that CESM coastal performance is broadly consistent with SST and oxygen

capacities during overlapping years. The forecasted and observed coastal oxygen capacities have similar latitudinal pattern.
315   These coastal results indicate more latitudinal pattern agreement between observations and model results than found for open-ocean oxygen concentrations at the thermocline (Oschlies et al., 2017). The CESM resolution, however, offers only a limited representation of coastal processes. Regional scales of variability are resolved, but smaller scales within estuaries are not. Research on future coastal oxygen conditions can be advanced with forecasts from local high-resolution models (Fennel and Testa, 2019), as for systems such as the Gulf of Mexico (Justic et al., 2007), Chesapeake Bay (Ni et al., 2019), and Baltic Sea
320   (Meier et al., 2019). Further steps forward will come as Earth system models improve resolution and the representation of physical and ecosystem processes in global coastal areas (e.g. Holt et al., 2009; Holt et al., 2017).

5 Conclusions

Linear trend analyses of a global 40-year observational gridded climate data record (updated from Merchant et al., 2019) and CESM 21st Century forecasts for the RCP 8.5 scenario indicate warming-related pressures on oxygen conditions are increasing.
325   The median trends forecasted along the global coast are 0.39 °C, -1.6 mmol m^{-3}, and -1.2 mmol m^{-3} per decade for SST, oxygen capacity, and oxygen concentration, respectively. These trends are considerably faster than the median forecasts for the entire surface ocean. The forecasted median coastal trends for SST and oxygen capacity are 48% and 18% faster than the corresponding observed rates. Significant portions of the global coast (upwards of 19%) are forecasted to change even more rapidly, with SST warming more than 0.60 °C per decade and oxygen capacity and concentrations rates faster than -3.0 mmol
330   m^{-3} per decade. Observed and forecasted rates tend to increase with latitude. Most (89%) of the documented hypoxic areas (Diaz et al., 2011) are in the mid-latitude (20-60 °N) northern hemisphere where trends tend to be larger, but not as extreme as coastal rates in the Arctic. The database documents only a few coastal hypoxic areas at high latitudes, where it is likely that new hypoxic areas will emerge due to warming and rapidly deteriorating oxygen conditions. Coastal megacities (at low and mid-latitudes) are likely to experience emerging or worsening hypoxia with the dual pressures of warming and increasing
335   populations. The forecasted warming and declining oxygen conditions will exert considerable pressure on current hypoxic areas, since future oxygen declines of any magnitude will have deleterious ecosystem effects as hypoxic intensity and duration worsens. The forecasted oxygen declines can erode oxygen gains achieved in systems improved by nutrient/wastewater management and should be incorporated into coastal environmental management strategies to protect future water quality and ecosystem services.

340   **Author contribution:** M.W. completed the research and wrote the manuscript.

Competing interests: The author declares that he has no conflict of interest.

References

345 Altieri, A. H. and Gedan, K. B.: Climate change and dead zones. *Global Change Biol.*, 21, 1395–1406, https://doi.org/10.1111/gcb.12754, 2015.

Bopp, L., Resplandy, L., Orr, J. C., Doney, S. C., Dunne, J. P., Gehlen, M., Halloran, P., Heinze, C., Ilyina, T., Séférian, R., Tjiputra, J., and Vichi, M.: Multiple stressors of ocean ecosystems in the 21st century: Projections with CMIP5 models. *Biogeosciences*, 10, 6225–6245, https://doi.org/10.5194/bg-10-6225-2013, 2013.

350 Beaufort Lagoon Ecosystems LTER: *Physiochemical water column parameters and hydrographic time series from river, lagoon, and open ocean sites along the Alaska Beaufort Sea coast*, 2018-ongoing ver 1. Environmental Data Initiative, https://doi.org/10.6073/pasta/e0e71c2d59bf7b08928061f546be6a9a, 2020.

Breitburg, D., Levin, L. A., Oschlies, A., Grégoire, M., Chavez, F. P., Conley, D. J., Garçon, V., Gilbert, D., Gutiérrez, D., Isensee, K., Jacinto, G. S., Limburg, K. E., Montes, I., Naqvi, S. W. A., Pitcher, G. C., Rabalais, N. N., Roman, M. R., Rose,
355 K. A., Seibel, B. A., Telszewski, M., Yasuhara, M., and Zhang, J.: Declining oxygen in the global ocean and coastal waters. *Science*, 359(6371), p.eaam7240, https://doi.org/10.1126/science.aam7240, 2018.

Brown, J. H., Gillooly, J. F., Allen, A. P., Savage, V. M., and West, G. B.: Toward a metabolic theory of ecology. *Ecology*, 85, 1771–1789, https://doi.org/10.1890/03-9000, 2004.

Cloern, J. E.: Our evolving conceptual model of the coastal eutrophication problem. *Mar. Ecol. Prog. Ser.*, 210, 223–253,
360 https://doi.org/10.3354/meps210223, 2001.

Cocco, V., Joos, F., Steinacher, M., Frölicher, T. L., Bopp, L., Dunne, J., Gehlen, M., Heinze, C., Orr, J., Oschlies, A., Schneider, B., Segschneider, J., and Tjiputra, J.: Oxygen and indicators of stress for marine life in multi-model global warming projections, *Biogeosciences*, 10, 1849-1868, https://doi.org/10.5194/bg-10-1849-2013, 2013.

Collins, W. D., Bitz, C. M., Blackmon, M. L., Bonan, G. B., Bretherton, C. S., Carton, J. A., Chang, P., Doney, S. C., Hack,
365 J. J., Henderson, T. B., Kiehl, J. T., Large, W. G., McKenna, D. S., Santer, B. D., and Smith, R. D.: The Community Climate System Model Version 3 (CCSM3). *J. Climate*, 19, 2122-2143, https://doi.org/10.1175/JCLI3761.1, 2006.

Diaz, R., Selman, M. and Chique, C.: *Global Eutrophic and Hypoxic Coastal Systems*. World Resources Institute. Eutrophication and Hypoxia: Nutrient Pollution in Coastal Waters. Available online at: https://datasets.wri.org/dataset/eutrophication-hypoxia-map-data-set, 2011.

370 Diaz R. J., and Rosenberg, R.: Spreading dead zones and consequences for marine ecosystems. *Science*, 321, 926–929, https://doi.org/10.1126/science.1156401, 2008.

Diaz, R.J. and Rosenberg, R.: Introduction to environmental and economic consequences of hypoxia. *Int. J. Water Resour. D.*, 27, 71-82, https://doi.org/10.1080/07900627.2010.531379, 2011.

Dommasnes, A., Rey, F., and Røttingen, I.: Reduced oxygen concentrations in herring wintering areas. *ICES J. Mar. Sci.*, 51,
375   63-69, https://doi.org/10.1006/jmsc.1994.1006, 1994.

Embury, O. and Good, S.: Sea surface temperature daily data from 1981 to present derived from satellite observations,
Level-4 Product. *Climate Data Store*, https://cds.climate.copernicus.eu/cdsapp#!/dataset/satellite-sea-surface-temperature,
2021.

Fennel, K. and Testa, J. M.: Biogeochemical controls on coastal hypoxia. *Ann. Rev. Mar. Sci.*, 11, 105-130,
380   https://doi.org/10.1146/annurev-marine-010318-095138, 2019.

Garcia, H. E., and Gordon, L. I.: Oxygen solubility in seawater: better fitting equations. *Limnol. Oceanogr.*, 37, 1307-1312,
https://doi.org/10.4319/lo.1992.37.6.1307, 1992.

Gilbert, D., Rabalais, N. N., Diaz, R. J., Zhang, J.: Evidence for greater oxygen decline rates in the coastal ocean than in the
open ocean. *Biogeosciences Discuss.*, 7, 2283-2296, https://doi.org/10.5194/bgd-6-9127-2009, 2010.

385   Hoegh-Guldberg, O., Jacob, D., Taylor, M., Bindi, M., Brown, S., Camilloni, I., Diedhiou, A., Djalante, R., Ebi, K. L.,
Engelbrecht, F., Guiot, J., Hijioka, Y., Mehrotra, S., Payne, A., Seneviratne, S. I., Thomas, A., Warren, R., Zhou, G., and
Tschakert, P.: Impacts of 1.5ºC Global Warming on Natural and Human Systems. In: *Global Warming of 1.5°C,* [Masson-
Delmotte, V., Zhai, P., Pörtner, H. -O., Roberts, D., Skea, J., Shukla, P. R., Pirani, A., Moufouma-Okia, W., Péan, C.,
Pidcock, R., Connors, S., Matthews, J. B. R., Chen, Y., Zhou, X., Gomis, M. I., Lonnoy, E., Maycock, T., Tignor, M., and
390   Waterfield, T. (eds.)], Geneva, Switzerland: World Meteorological Organization, https://www.ipcc.ch/sr15/chapter/chapter-
3/, 2018.

Holt, J., Harle, J., Proctor, R., Michel, S., Ashworth, M., Batstone, C., Allen, I., Holmes, R., Smyth, T., Haines, K.,
Bretherton, D., and Smith, G.: Modelling the global coastal ocean. *Philosophical Transactions of the Royal Society A:
Mathematical, Physical and Engineering Sciences*, 367(1890), 939-951, https://doi.org/10.1098/rsta.2008.0210, 2009.

395   Holt, J., Hyder, P., Ashworth, M., Harle, J., Hewitt, H. T., Liu, H., New, A. L., Pickles, S., Porter, A., Popova, E., Allen, J.
I., Siddorn, J., and Wood, R.: Prospects for improving the representation of coastal and shelf seas in global ocean models.
Geosci. Model Dev., 10, 499-523, https://doi.org/10.5194/gmd-10-499-2017, 2017.

Justic, D., Bierman, V. J., Scavia, D., and R. D. Hetland, R. D.: Forecasting Gulf's Hypoxia: The Next 50 Years? *Estuar.
Coasts*, 30, 791-801, https://doi.org/10.1007/BF02841334, 2007.

400   Kay, J. E., Deser, C., Phillips, A., Mai, A., Hannay, C., Strand, G., Arblaster, J., Bates, S., Danabasoglu, G., Edwards, J.,
Holland, M., Kushner, P., Lamarque, J. -F., Lawrence, D., Lindsay, K., Middleton, A., Munoz, E., Neale, R., Oleson, K.,
Polvani, L., and Vertenstein, M.: The Community Earth System Model (CESM) Large Ensemble Project: A Community
Resource for Studying Climate Change in the Presence of Internal Climate Variability, *B. Am. Meteorol. Soc.*, 96, 1333-
1349. https://doi.org/10.1175/BAMS-D-13-00255.1, 2015a.

405 Kay, J. E., Deser, C., Phillips, A., Mai, A., Hannay, C., Strand, G., Arblaster, J., Bates, S., Danabasoglu, G., Edwards, J., Holland, M., Kushner, P., Lamarque, J. -F., Lawrence, D., Lindsay, K., Middleton, A., Munoz, E., Neale, R., Oleson, K., Polvani, L., and Vertenstein, M.: CESM1 CAM5 BGC 20C + RCP8.5 Large Ensemble, *Earth System Grid*, https://www.earthsystemgrid.org/dataset/ucar.cgd.ccsm4.cesmLE.html, 2015b.

Meier, H. E. M., Eilola, K., Almroth-Rosell, E., Schimanke, S., Kniebusch, M., Höglund, A., Pemberton, P., Liu, Y., Väli,
410 G., Saraiva, S.: Disentangling the impact of nutrient load and climate changes on Baltic Sea hypoxia and eutrophication since 1850. *Clim. Dynam.*, 53, 1145–1166, https://doi.org/10.1007/s00382-018-4296-y, 2019.

Melillo, J. M., Richmond, T. C., and Yohe, G. W. (eds.): *Climate Change Impacts in the United States: The Third National Climate Assessment*. U.S. Global Change Research Program, 841 pp. https://doi.org/10.7930/J0Z31WJ2, 2014.

Merchant, C. J., O. Embury, C. E. Bulgin, T. Block, G. K. Corlett, E. Fiedler, S. A. Good, J. Mittaz, N. A. Rayner, D. Berry,
415 S. Eastwood, M. Taylor, Y. Tsushima, A. Waterfall, R. Wilson, and C. Donlon: Satellite-based time-series of sea surface temperature since 1981 for climate applications. *Nature, Scientific Data*, 6:223, 18 pp., https://doi.org/10.1038/s41597-019-0236-x, 2019.

Moss, R. H., Edmonds, J. A., Hibbard, K. A., Manning, M. R., Rose, S. K., van Vuuren, D. P., Carter, T. R., Emori, S., Kainuma, M., Kram, T., Meehl, G. A., Mitchell, J. F. B., Nakicenovic, N., Riahi, K., Smith, S. J., Stouffer, R. J., Thomson,
420 A. M., Weyant, J. P., and Wilbanks, T. J.: The next generation of scenarios for climate change research and assessment. *Nature*, 463(7282), 747-756, https://doi.org/10.1038/nature08823, 2010.

Nakicenovic, N. and Swart, R. (eds.): *Emission Scenarios: Intergovernmental Panel on Climate Change Special Report on Emission Scenarios*, Cambridge University Press, 570 pp., https://www.ipcc.ch/site/assets/uploads/2018/03/emissions_scenarios-1.pdf, 2000.

425 Ni, W., M. Li, M., Ross, A. C., and Najjar, R. G.: Large Projected Decline in Dissolved Oxygen in a Eutrophic Estuary Due to Climate Change. *J. Geophys. Res.: Oceans*, 124, 8271-8289, https://doi.org/10.1029/2019JC015274, 2019.

Oschlies, A., Duteil, O., Getzlaff, J., Koeve, W., Landolfi, A., Schmidtko, S.: Patterns of deoxygenation: sensitivity to natural and anthropogenic drivers. *Phil. Trans. R. Soc. A*, 375, 20160325. https://doi.org/10.1098/rsta.2016.0325, 2017.

Paerl, H. W.: Assessing and managing nutrient-enhanced eutrophication in estuarine and coastal waters: Interactive effects of
430 human and climatic perturbations. *Ecol. Eng.*, 26, 40-54, https://doi.org/10.1016/j.ecoleng.2005.09.006, 2006.

Pershing, A.J., Alexander, M. A., Hernandez, C. M., Kerr, L. A., Le Bris, A., Mills, K. E., Nye, J. A., Record, N. R., Scannell, H. A., Scott, J. D., Sherwood, G. D., and Thomas, A. C.: Slow adaptation in the face of rapid warming leads to collapse of the Gulf of Maine cod fishery. *Science*, 350(6262), 809-812, https://doi.org/10.1126/science.aac9819, 2015.

Rabalais, N.N. and Turner, R. E. (Eds.): *Coastal Hypoxia: Consequences for Living resources and Ecosystems*. Coastal and
435   Estuarine Studies 58. American Geophysical Union, Washington, DC, 454 pp., https://doi.org/10.1029/CE058, 2001.

Rabalais, N. N., Diaz, R. J., Levin, L. A., Turner, R. E., Gilbert, D., and Zhang, J.: Dynamics and distribution of natural and
human-caused hypoxia. *Biogeosciences*, 7, 585–619, https://doi.org/10.5194/bg-7-585-2010, 2010.

Smith, S. D.: *Chemical Parameters of Northern Alaska Coastal Lagoons*. Unpublished term paper for CE 394K: GIS in
Water Resources (D. Maidment), University of Texas, 23 pp,
440   https://www.caee.utexas.edu/prof/maidment/giswr2012/TermPaper/Smith.pdf, 2012.

Taylor, K. E., Stouffer, R. J., and Meehl, G. A.: An overview of CMIP5 and the experiment design. *B. Am. Meteorol. Soc.*,
93, 485-498, https://doi.org/10.1175/BAMS-D-11-00094.1, 2012.

Vaquer-Sunyer, R. and Duarte, C. M.: Thresholds of hypoxia for marine biodiversity, *PNAS*, 105, 15452–15457,
https://doi.org/10.1073/pnas.0803833105, 2008.

445   Varis, O., Biswas, A. K., Tortajada, C., and Lundqvist, J.: Megacities and Water Management, *Water Res. Dev.*, 22:2, 377-
394, https://doi.org/10.1080/07900620600684550, 2006.

von Glasow, R., Jickells, T. D., Baklanov, A., Carmichael, G. R., Church, T. M., Gallardo, L., Hughes, C., Kanakidou, M.,
Liss, P. S., Mee, L. and Raine, R.: Megacities and large urban agglomerations in the coastal zone: interactions between
atmosphere, land, and marine ecosystems. *Ambio*, 42(1), 13-28, https://doi.org/10.1007/s13280-012-0343-9, 2013.

450   Weiss R. F.: Solubility of nitrogen, oxygen and argon in water and seawater. *Deep-Sea Res.*, 17, 721–735,
https://doi.org/10.1016/0011-7471(70)90037-9, 1970.

Whitney, M. M.: Supporting dataset for observed and forecasted global warming pressure on coastal hypoxia. Department of
Marine Sciences, *OpenCommons@UConn*, https://opencommons.uconn.edu/marine_sci/13, 2021.